Linear-Phase Approximation in the Triangular Facet Near-Field Physical Optics Computer Program

W. A. Imbriale and R. E. Hodges
Ground Antennas and Facilities Engineering Section

Analyses of reflector antenna surfaces use a computer program based on a discrete approximation of the radiation integral. The calculation replaces the actual surface with a triangular facet representation; the physical optics current is assumed to be constant over each facet. This article describes a method of calculation using linear-phase approximation of the surface currents of parabolas, ellipses, and shaped subreflectors and compares results with a previous program that used a constant-phase approximation of the triangular facets. The results show that the linear-phase approximation is a significant improvement over the constant-phase approximation, and enables computation of 100–1,000λ reflectors within a reasonable time on a Cray computer.

I. Introduction

One of the simplest reflector antenna computer programs is based on a discrete approximation of the radiation integral. This calculation replaces the actual reflector surface with a triangular facet representation so that the reflector resembles a geodesic dome. The physical optics (PO) current is assumed to be constant in magnitude and phase over each facet, so the radiation integral is reduced to a simple summation. This program has proven to be surprisingly robust and useful for the analysis of small reflectors, particularly when the near-field is desired and surface derivatives are not known.

It is natural to inquire whether a more sophisticated approximation of the PO surface current will yield more accurate results or permit the use of larger facets. In this article, a linear-phase approximation of the surface current is made. Within each triangular region, the resulting integral is the two-dimensional Fourier transform of the projected triangle. This triangular-shape function integral can be computed in closed form [1]. The complete PO integral is then a summation of these transforms.

Once the current on the triangle is determined, the linear-phase approximation takes about three times longer to compute a field point than does the constant-phase approximation. Thus the time savings depend on reducing the number of triangles required to achieve convergence.

Examples are given for scattering from parabolas, ellipses, and shaped surfaces. The general trend is similar for all cases in that, depending upon the size of the triangles, there is an angular limit over which the solution is valid. This angular limit is significantly larger with the linear-phase approximation than with the constant-phase approximation. Thus the linear-phase approximation can be used to solve larger problems if core limitations are a

problem, or alternatively, a smaller number of triangles can be used to solve the same size problem.

II. Analytical Details

The PO radiation integral over the reflector surface Σ can be expressed [2]

$$\mathbf{H}(\mathbf{r}) = -\frac{1}{4\pi}\int_{\Sigma}\left(jk+\frac{1}{R}\right)\hat{\mathbf{R}}\times\mathbf{J}_s(\mathbf{r}')\frac{e^{-jkR}}{R}ds' \quad (1)$$

in which $\mathbf{r}$ designates the field point, $\mathbf{r}'$ the source point, $R = |\mathbf{r}-\mathbf{r}'|$ is the distance between them, and $\hat{\mathbf{R}} = (\mathbf{r}-\mathbf{r}')/R$ is a unit vector. The PO surface current on the subreflector surface $\mathbf{J}_s$ is expressed

$$\mathbf{J}_s(\mathbf{r}') = 2\hat{\mathbf{n}}\times\mathbf{H}_s(\mathbf{r}') \quad (2)$$

For the purpose of analysis, the true surface Σ is replaced by a contiguous set of N-plane triangular facets. These facets, denoted Δ_i, are chosen to be roughly equal in size with their vertices on the surface Σ. Figure 1 shows a typical facet and its projection onto the x-y plane. Let (x_i, y_i, z_i) represent the *centroid* of each triangle where the subscript $i = 1, \cdots, N$ is associated with a triangle. Then, the field obtained by replacing the true surface Σ by the triangular facet approximation is

$$\mathbf{H}(\mathbf{r}) = -\frac{1}{4\pi}\sum_{i=1}^{N}\int_{\Delta_i}\left(jk+\frac{1}{R}\right)\hat{\mathbf{R}}\times\mathbf{J}(\mathbf{r}')\frac{e^{-jkR}}{R}ds' \quad (3)$$

In Eq. (3), $\mathbf{J}$ is now the equivalent surface current evaluated on the triangular facets. Since the triangles are small, it is expected that $\hat{\mathbf{R}}$ and R do not vary appreciably over the area of a given facet. Thus, let $\hat{\mathbf{R}}_i$ and R_i be the value obtained at the centroid (x_i, y_i, z_i) of each facet and approximate Eq. (3) by

$$\mathbf{H}(\mathbf{r}) = -\frac{1}{4\pi}\sum_{i=1}^{N}\left(jk+\frac{1}{R_i}\right)\hat{\mathbf{R}}_i\times\mathbf{T}_i(\mathbf{r}) \quad (4)$$

$$\mathbf{T}_i(\mathbf{r}) = \int_{\Delta_i}\mathbf{J}_i(\mathbf{r}')\frac{e^{-jkR}}{R_i}ds' \quad (5)$$

Assume that the necessary transformations have been performed so that the incident field $\mathbf{H}_s$ is given in terms of the reflector coordinate system. Then

$$\mathbf{J}_i(\mathbf{r}') = 2\hat{\mathbf{n}}_i\times\mathbf{H}_s(\mathbf{r}') \quad (6)$$

Next, assume that the incident field can be represented by a function of the form

$$\mathbf{H}_s = \mathbf{h}_s(\mathbf{r}_i)\frac{e^{-jkr_s}}{4\pi r_{si}} \quad (7)$$

where r_s is the distance to the source point. Then, Eq. (5) can be written

$$\mathbf{T}_i(\mathbf{r}) = \frac{\hat{\mathbf{n}}_i\times\mathbf{h}_s(\mathbf{r}_i)}{2\pi R_i r_{si}}\int_{\Delta_i}e^{-jk(R+r_s)}ds' \quad (8)$$

To simplify the form of the integration, the surface Jacobian is introduced within each triangular facet Δ_i. For a planar surface $z_i = f_i(x, y)$, a normal is given by

$$\mathbf{N}_i = -\hat{\mathbf{x}}f_{xi} - \hat{\mathbf{y}}f_{yi} + \hat{\mathbf{z}} \quad (9)$$

where

$$f_{xi} \equiv \frac{\partial f_i}{\partial x} \qquad f_{yi} \equiv \frac{\partial f_i}{\partial y}$$

and a unit normal is given by

$$\hat{\mathbf{n}}_i = \frac{\mathbf{N}_i}{|\,\mathbf{N}_i\,|} \quad (10)$$

This permits the explicit evaluation of the Jacobian as

$$J_{\Delta_i} = |\,\mathbf{N}_i\,| = \left[f_{xi}^2 + f_{yi}^2 + 1\right]^{1/2} \quad (11)$$

Making use of the Jacobian then allows Eq. (8) to be rewritten as

$$\mathbf{T}_i(\mathbf{r}) = \frac{\hat{\mathbf{n}}_i\times\mathbf{h}_s(\mathbf{r}_i)}{2\pi R_i r_{si}}J_{\Delta_i}\int_{\Delta_i'}e^{-jk(R+r_s)}dx'dy' \quad (12)$$

in which Δ_i' represents the area of the ith triangular facet projected onto the $z = 0$ plane. Now, make a Taylor-series expansion of the exponent in Eq. (12). Retaining only the first-order terms, one can formally write

$$R(x, y) + r_s(x, y) = \frac{1}{k}(a_i - u_i x - v_i y) \quad (13)$$

in which a_i, u_i, and v_i are constants. This approximation corresponds to a far-field approximation on the ith triangle. With this approximation, Eq. (12) reduces to

$$\mathbf{T}_i(\mathbf{r}) = \frac{\hat{\mathbf{n}}_i \times \mathbf{h}_s(\mathbf{r}_i)}{2\pi R_i r_{si}} J_{\Delta_i} e^{-ja_i} \int_{\Delta_i'} e^{j(u_i x' + v_i y')} dx'dy' \quad (14)$$

It may now be observed that this integral is the two-dimensional Fourier transform of the ith projected triangle Δ_i', expressed as

$$S(u,v) = \int_{\Delta_i'} e^{j(ux+vy)} dxdy \quad (15)$$

In order to explicitly evaluate the constants in Eq. (13), note that the equation of a plane can be expressed as

$$z = (x - x_i) f_{xi} + (y - y_i) f_{yi} + z_i$$

This can be used to obtain

$$a_i = kR(x_i, y_i) + kr_s(x_i, y_i) + u_i x_i + v_i y_i \quad (16)$$

$$\frac{u_i}{k} = \frac{(x_p - x_i) + (z_p - z_i) f_{xi}}{R(x_i, y_i)} + \frac{(x_s - x_i) + (z_s - z_i) f_{xi}}{r_s(x_i, y_i)} \quad (17)$$

$$\frac{v_i}{k} = \frac{(y_p - y_i) + (z_p - z_i) f_{yi}}{R(y_i, y_i)} + \frac{(y_s - y_i) + (z_s - z_i) f_{yi}}{r_s(y_i, y_i)} \quad (18)$$

Placing the result of Eq. (16) into Eq. (14), and recalling Eqs. (6) and (7), yields

$$\mathbf{T}_i(\mathbf{r}) = \mathbf{J}_i(r_i) J_{\Delta_i} e^{-j(u_i x_i + v_i y_i)} S(u_i, v_i) \frac{e^{-jkR_i}}{R_i} \quad (19)$$

This is the final form of the linear-phase approximation over each triangular facet. This expression can be used in Eq. (4) to compute the radiation integral once the Fourier transform of a triangular shape function $S(u,v)$ is known. Fortunately, this transform can be computed in closed form [1] from the expression

$$S(u,v) = \sum_{n=1}^{3} e^{j(ux_n + vy_n)} \frac{p_{n-1} - p_n}{(u + p_{n-1}v)(u + p_n v)} \quad (20)$$

in which (x_n, y_n) are the coordinates of the triangle vertices numbered in a clockwise direction. The slope of the nth side (between corners n and $n+1$) is given by

$$p_n = \frac{y_{n+1} - y_n}{x_{n+1} - x_n} \quad (21)$$

Some attention must be given to the following special cases. First, if $u = v = 0$, the transform reduces to the formula for the area of a triangle

$$S(0,0) = -\frac{1}{2}\Big[x_1(y_2 - y_3) + x_2(y_3 - y_1) + x_3(y_1 - y_2)\Big] \quad (22)$$

Next, if $u/v \to -p_n$, then

$$\lim_{u/v \to -p_n} S(u,v) = \frac{p_{n+1} - p_{n-1}}{v^2(p_{n+1} - p_n)(p_{n-1} - p_n)} \times \Big[e^{j(ux_{n-1} + vy_{n-1})} - e^{j(ux_n + vy_n)}\Big] + \frac{(x_{n+1} - x_n)}{jv} e^{j(ux_n + vy_n)} \quad (23)$$

III. Numerical Results

A FORTRAN subroutine was written to perform the linear-phase calculations indicated above. Test cases were run for parabolas, ellipses, and shaped subreflectors, and the results were compared with the previous program, which used a constant magnitude and phase approximation on the triangular facets. A focused parabola is neither an interesting nor a challenging case for the algorithm, since the phase variation over the facet is small. As a simple test case, the far-field pattern and gain of a $1,000\lambda$-diameter parabolic reflector with a focal length of $F = 400\lambda$ was calculated. The reflector is illuminated by a linearly polarized horn with a $\cos\theta$ pattern function. Figure 2 compares the linear- and constant-phase approximation for a roughly equally spaced 80-by-80 rectangular grid of points divided into triangles over the reflector surface (approximately 10,000 triangles). The running time on a Cray X-MP was less than one minute. It has been previously demonstrated [3,4,5] that, once sufficient triangles to converge the solution have been utilized, the results of the constant-phase algorithm are valid, so only comparisons of the two techniques are presented.

A more interesting example is the ellipse shown in Fig. 3. The projected aperture of the ellipse is about 3 m, illumination function is a $\cos^{42}\theta$ pattern function (22.3-dB gain), and the frequency is 31.4 GHz. The ellipse is about 350λ along the major axis. Figure 4 compares the constant-phase approximation for different grid densities of approximately 4,000, 10,000, and 23,000 triangles and illustrates a general trend of the method, i.e., depending on the size of the triangles, there is an angular limit over

which the solution is valid. Figure 5 compares the linear-phase approximation with the constant-phase approximation for the 4,000-triangle case and demonstrates that the angular range is larger with the linear-phase approximation.

A third example is the shaped subreflector shown in Fig. 6. The diameter is 3.42 m (135 in.), and it is fed with a $\cos^{233}\theta$ pattern function (29.7-dB gain). Figure 7 compares the results of a 4,000- and 10,000-triangle grid constant-phase approximation with a 4,000-triangle linear-phase approximation. The frequency of operation is 2.3 GHz, hence, the subreflector is about 26λ in diameter. The 10,000-triangle constant phase is the converged result, and the 4,000-triangle linear case gives the same result. A very good approximation is also obtained with a 1,400-triangle grid for the linear case, but no meaningful results are obtained with the constant-phase case. Figure 8 gives the linear-phase result for 31.4 GHz (360λ subreflector) using 23,000 triangles. No meaningful result is obtained for the equivalent constant-phase case.

Most of the examples given are for large reflectors to illustrate the robust character of the technique. For smaller reflectors ($< 100\lambda$), meaningful results can be obtained on a PC in a reasonable time.

IV. Conclusions

The linear-phase approximation is a significant improvement over the constant-phase approximation and enables the computation of fairly large (100 to $1,000\lambda$) reflectors in a reasonable time (on the order of minutes) on a Cray computer.

References

[1] S. W. Lee and R. Mittra, "Fourier Transform of a Polygonal Shape Function and Its Application in Electromagnetics," *IEEE Trans. Antennas and Propagation*, vol. 31, no. 1, pp. 99–103, January 1983.

[2] A. W. Rudge, K. Milne, A. D. Olver, and P. Knight, *The Handbook of Antenna Design, Vol. I*, London: Peter Peregrinus, 1982.

[3] V. Galindo-Israel, T. Veruttipong, and W. Imbriale, "GTD, Physical Optics and Jacobi-Bessel Diffraction Analysis of Beamwaveguide Ellipsoids," *AP-S International Symposium*, Philadelphia, Pennsylvania, pp. 643–646, 1986.

[4] T. Veruttipong, J. R. Withington, V. Galindo-Israel, W. A. Imbriale, and D. A. Bathker, "Design Considerations for Beamwaveguide in the NASA Deep Space Network," *IEEE Trans. Antennas and Propagation*, vol. AP-36, no. 12, pp. 1779–1787, December 1988.

[5] A. G. Cha and W. A. Imbriale, "New Analysis of Beamwaveguide Antennas Considering the Presence of the Metallic Tube and Its Experimental Verification," *AP-S International Symposium*, Dallas, Texas, pp. 1506–1509, 1990.

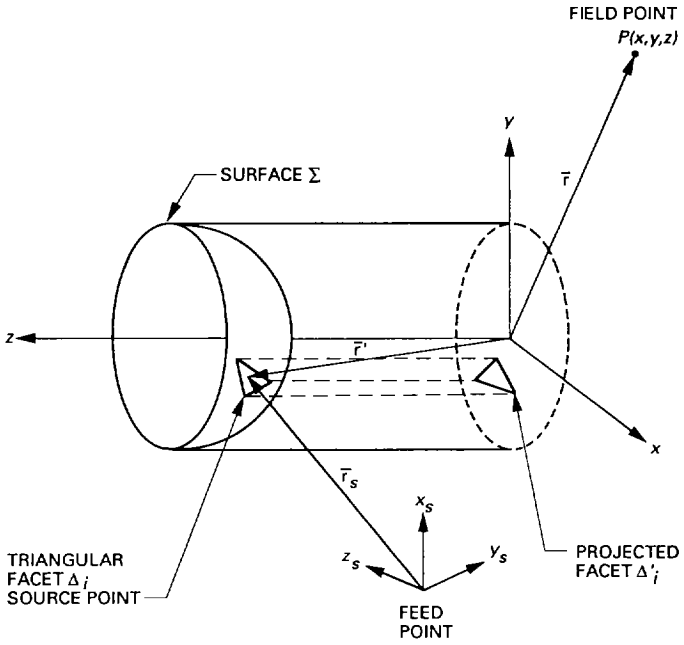

Fig. 1. Reflector analysis coordinate systems and a typical triangular facet.

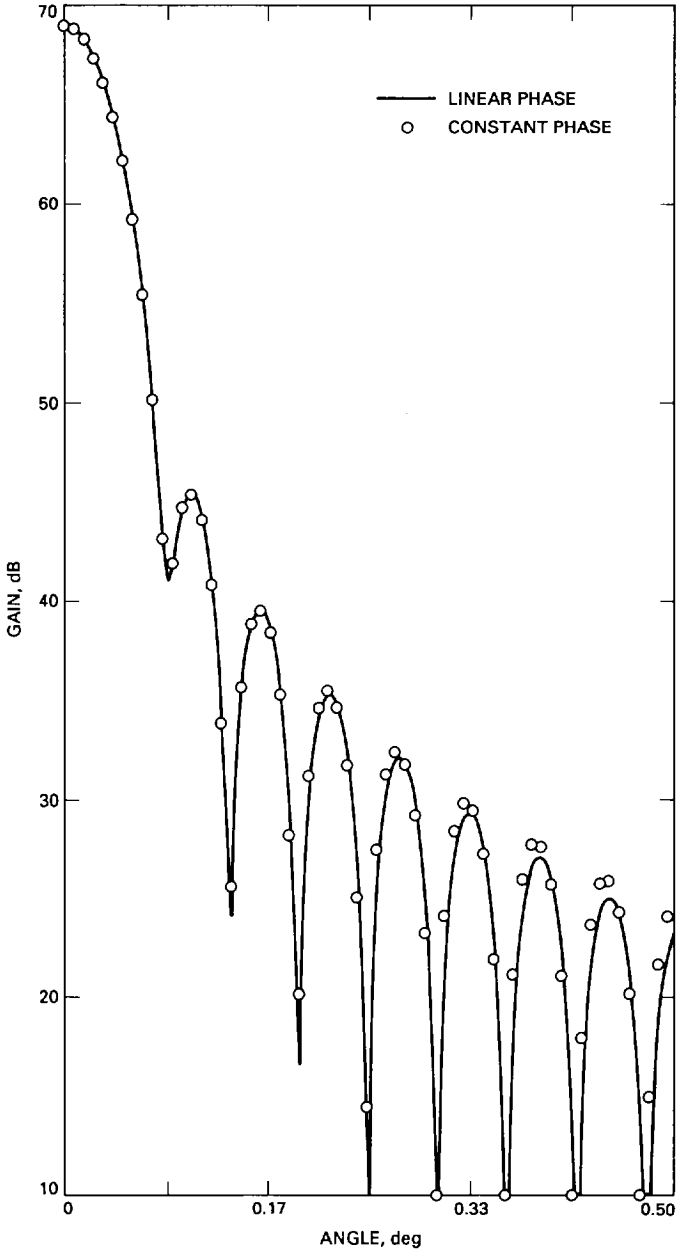

Fig. 2. Parabolic example.

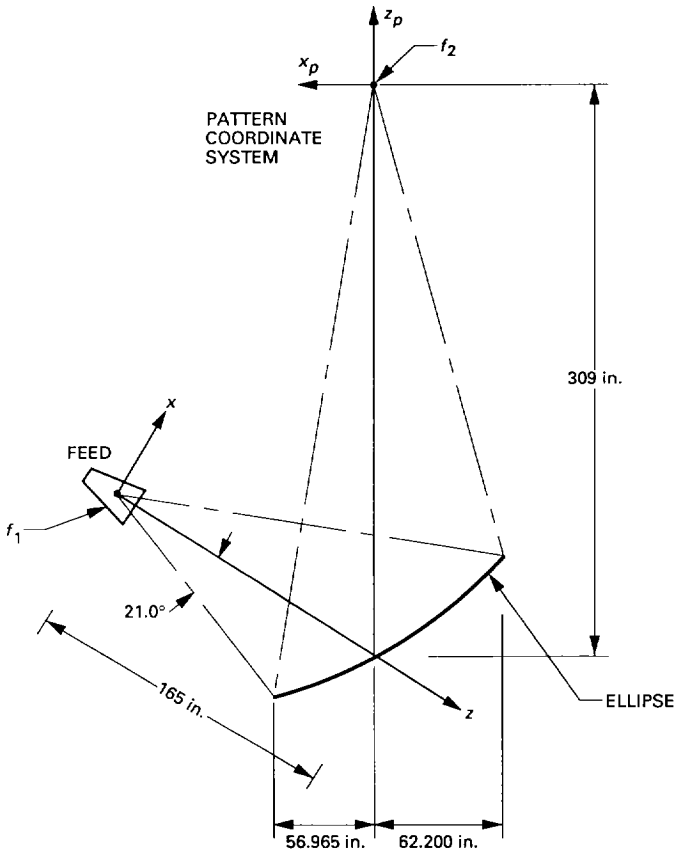

Fig. 3. Ellipse geometry.

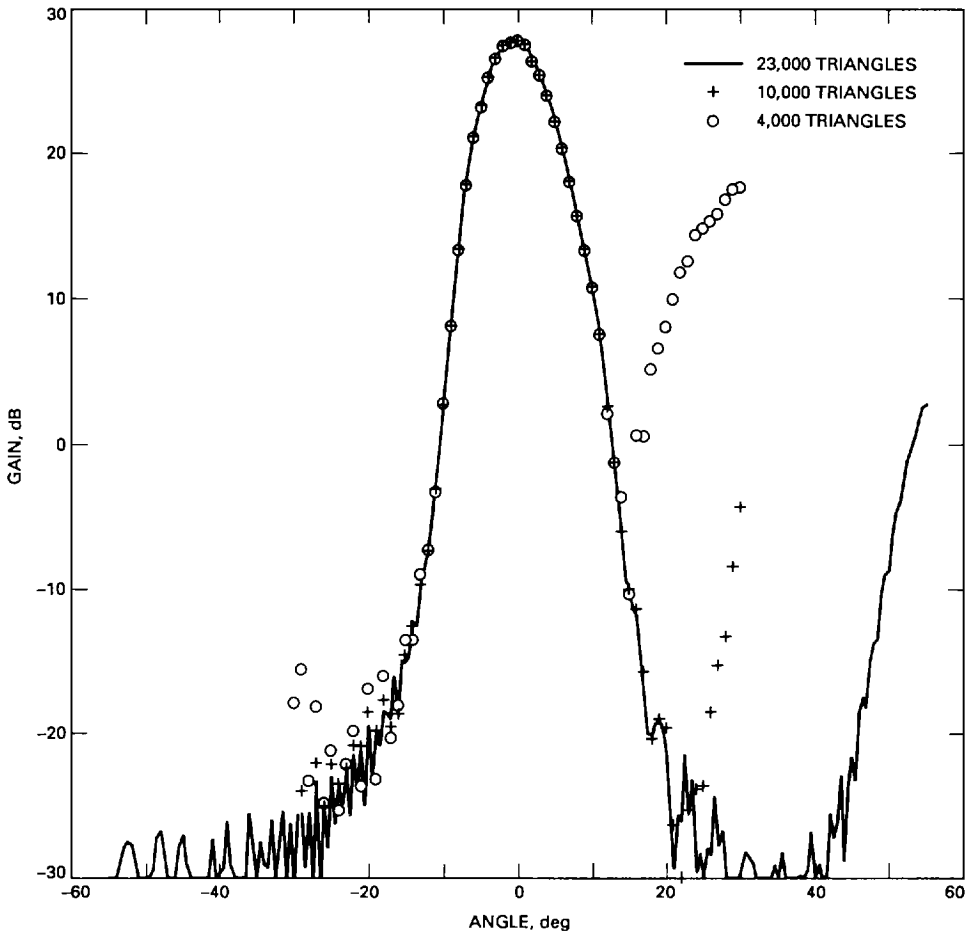

Fig. 4. Ellipse example: constant-phase approximation for offset plane.

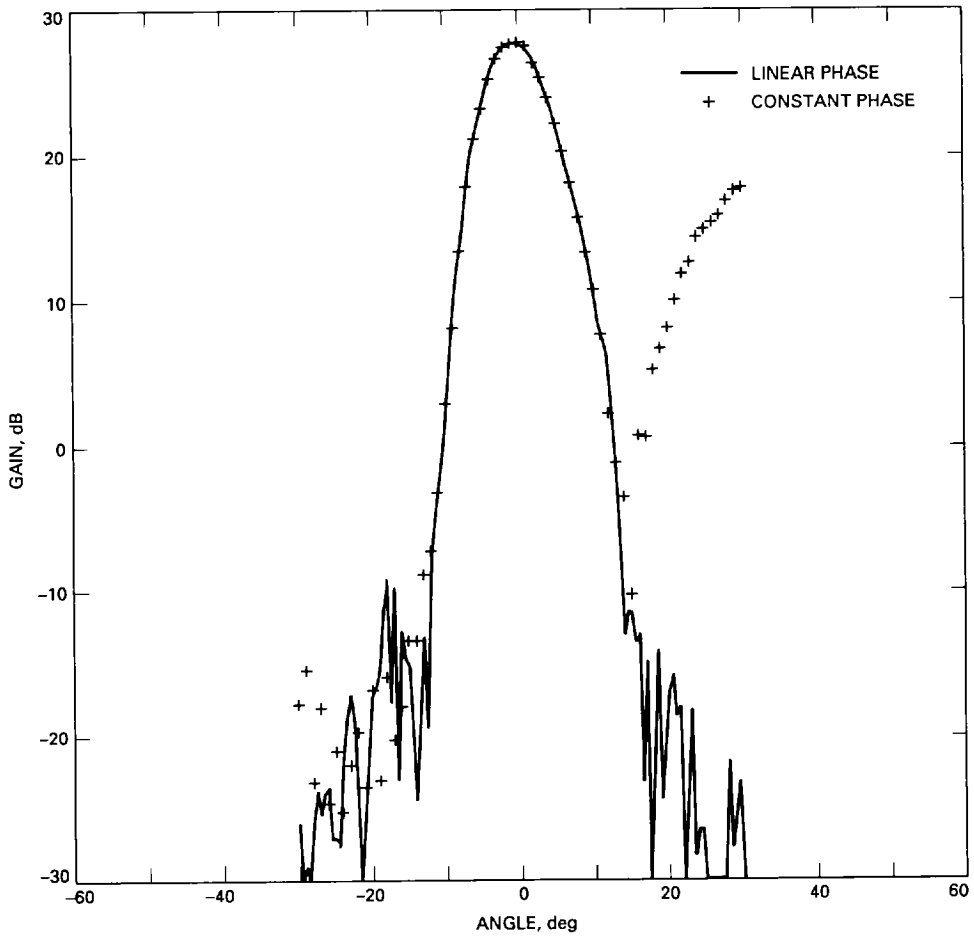

Fig. 5. Ellipse example: constant versus linear phase for offset plane.

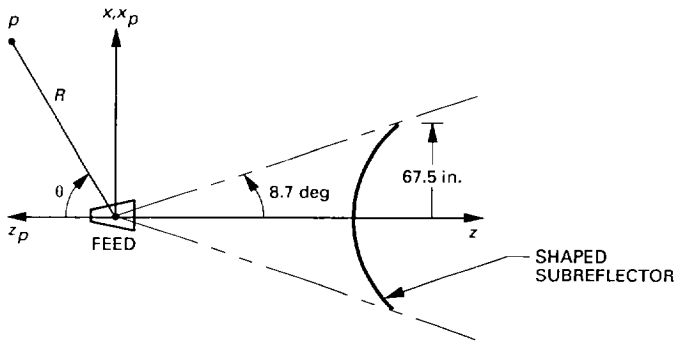

Fig. 6. Shaped subreflector geometry.

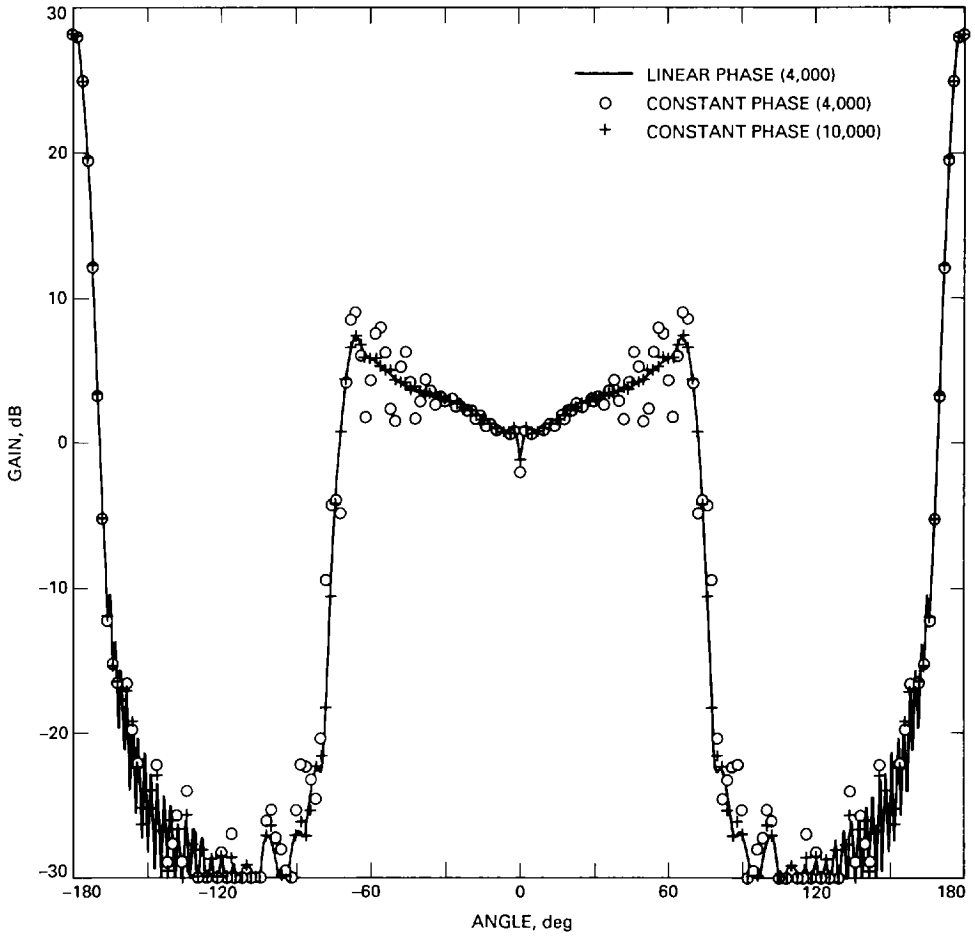

Fig. 7. Shaped subreflector example for H-plane at 2.3 GHz.

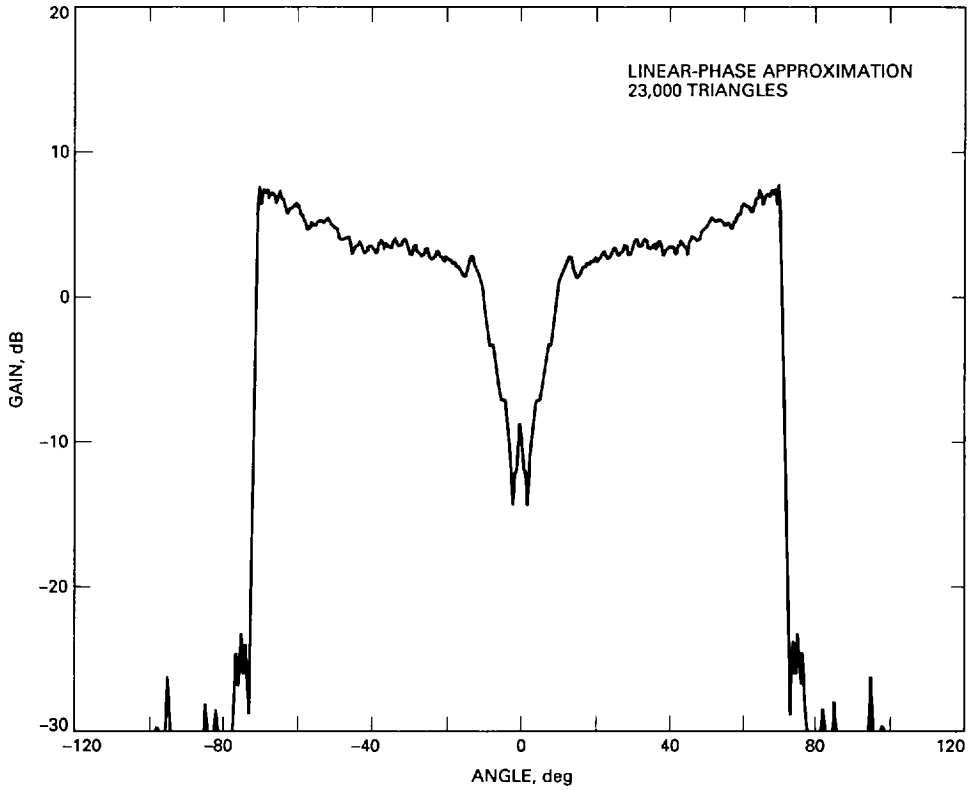

Fig. 8. Shaped subreflector, 31.4 GHz.